Supporting Information

Photo-controlled reversible secondary self-assembly of supramolecular nanosheets and their drug delivery behavior

*Ting Zhang and Chun-Hua Zhang**

MIIT Key Laboratory of Critical Materials Technology for New Energy Conversion and Storage, School of Chemistry and Chemical Engineering, Harbin Institute of Technology, P. O. Box 1254, Harbin, 150001, P. R. China, zhangchunhua@hit.edu.cn

Contents

1. General Information.

^{1}H NMR, ^{13}C NMR spectra, COSY and ROESY were recorded on a Bruker AVANCE AV400 (400 MHz and 100 MHz). The residual ^{1}H peak of deuterated solvent appeared at 4.79 ppm in D_2O, at 7.26 ppm in $CDCl_3$. UV/vis spectra and optical transmittance were recorded on a Shimadzu UV-3600 spectrophotometer equipped with a PTC-348 WI temperature controller. Solid-state fluorescence emission spectra were measured on an Edinburgh Instruments Fluorescence Spectrometer FS5 and quantum yield measurements were measured on a FLS 920P fluorescence spectroscopy. The dynamic light scattering (DLS) was measured by Brookhaven Instruments at 25 ℃. The samples for TEM measurement were prepared by dropping the solution onto a copper grid. The grid was then air-dried. The samples were examined by a Philips EM400st transmission electron microscope. The samples for SEM were prepared by dropping the solution on conductive glass, then air-dried and recorded on a JEOL JSM-7500F scanning electronic microscope operating at an accelerating voltage of 30 k eV. ESI-MS were measured by Agilent 6520 Q-TOF-MS. UV light (365 nm) source come from portable UV detection lamp and 420 nm light source from CEL-HXF300/CEL-HXUV300 Beijing AuLight Company. The Job plot were obtained by UV-vis absorption spectrum of the different ratios of the host and the guest changed from 1:9 to 9:1. The total concentration was 0.05 mM. The association binding constant K were measured by UV-vis absorption spectral titration from 1:0 to 1:1.5. According to the related formulas, the bonding constant was obtained by the nonlinear least square method.

2. Synthesis of the compounds.

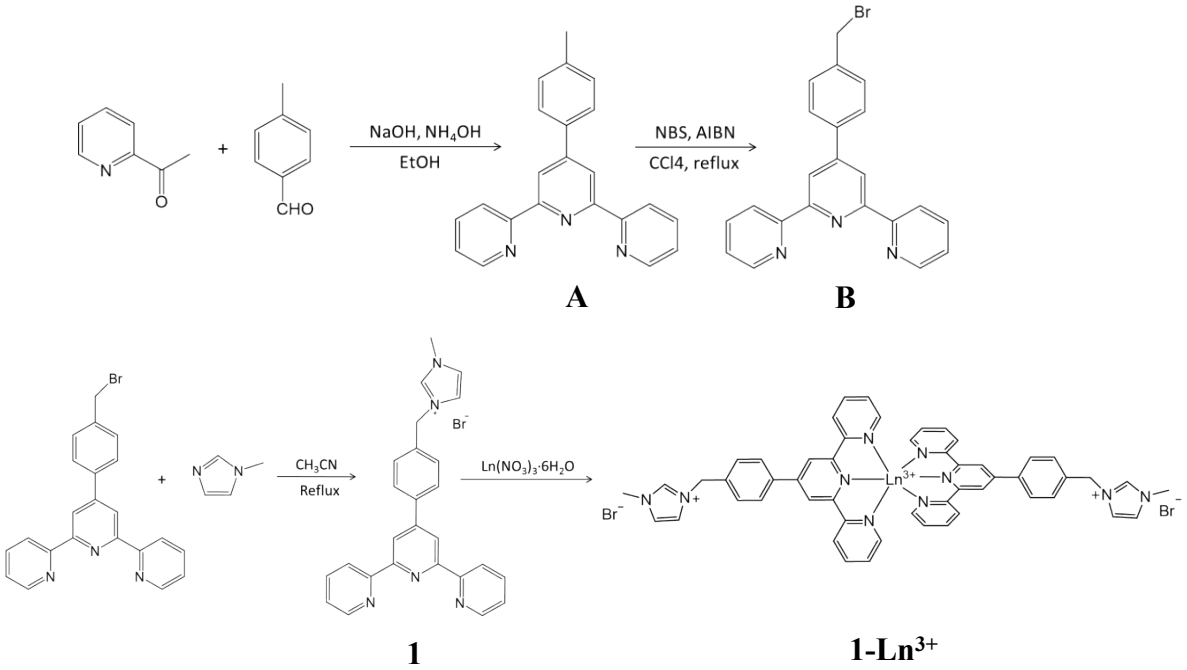

Scheme S1. Synthetic routes of compounds **A**, **B** and **1**.

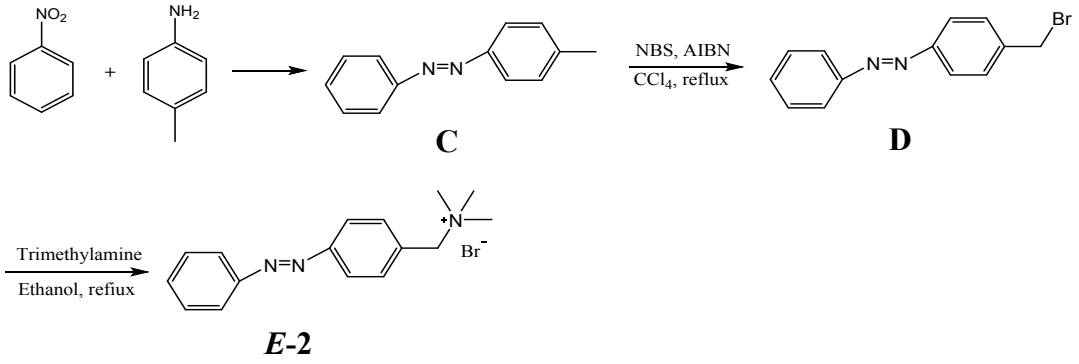

Scheme S2. Synthetic routes of compounds **C**, **D** and ***E*-2**.

3. NMR and MS spectra of the compounds.

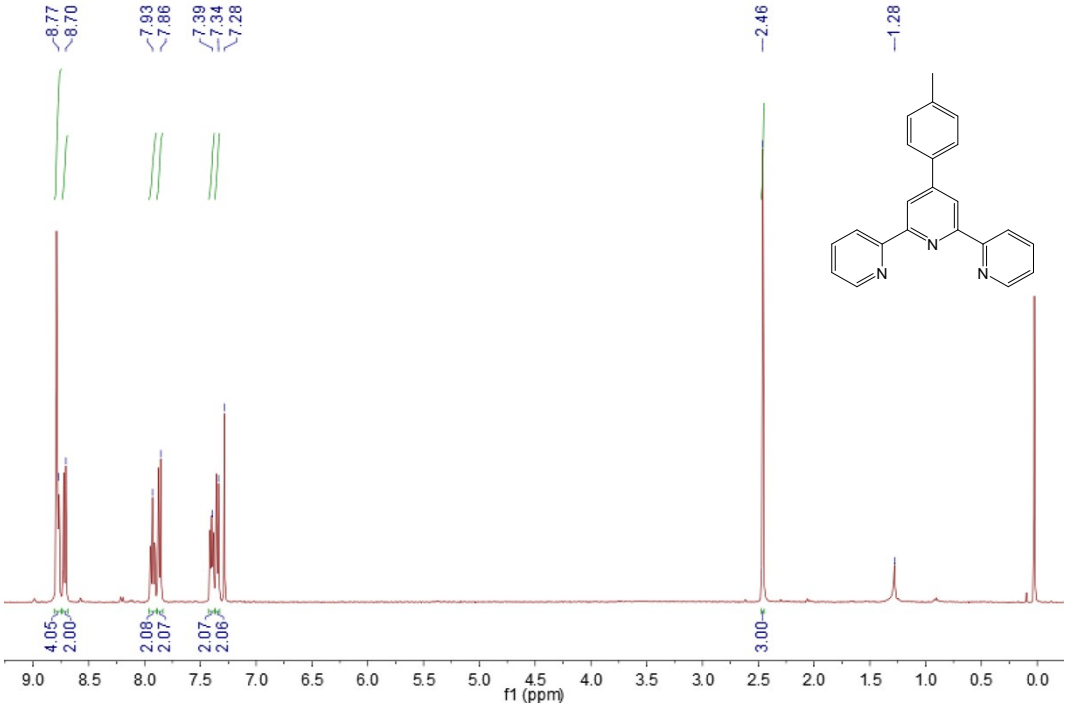

Fig. S1 ^{1}H NMR spectrum (400 MHz, $CDCl_3$) of compound **A** at 298 K.

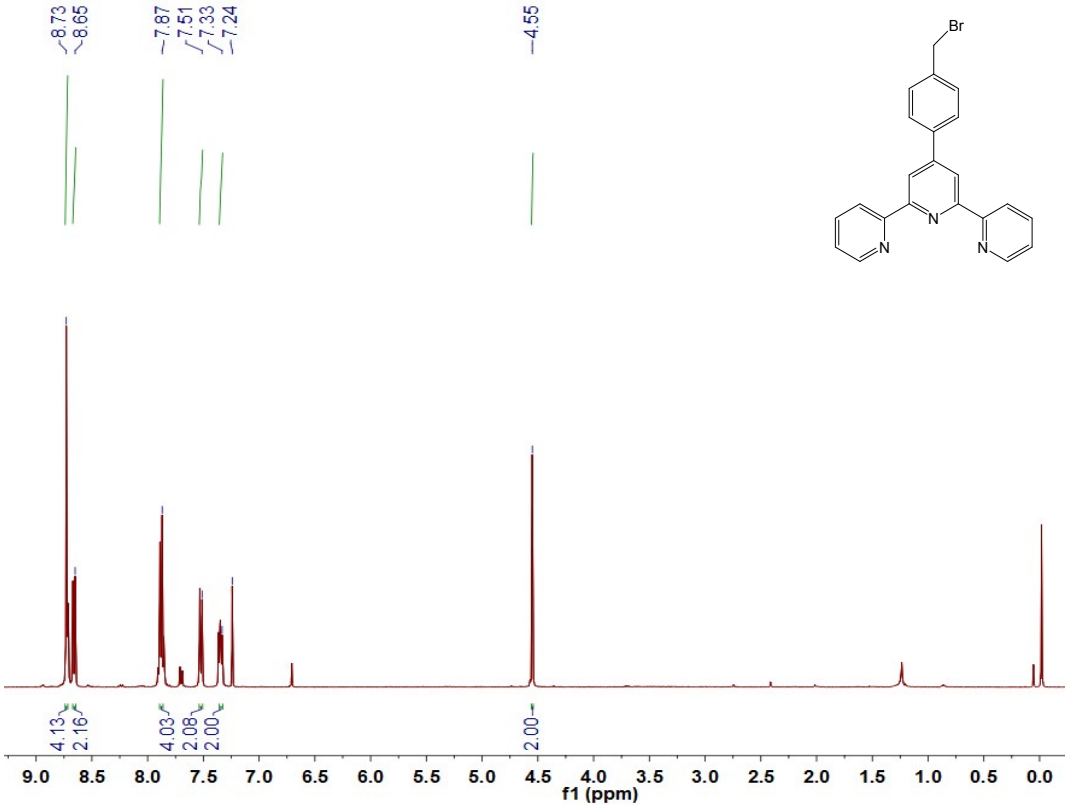

Fig. S2 ^{1}H NMR spectrum (400 MHz, $CDCl_3$) of compound **B** at 298 K.

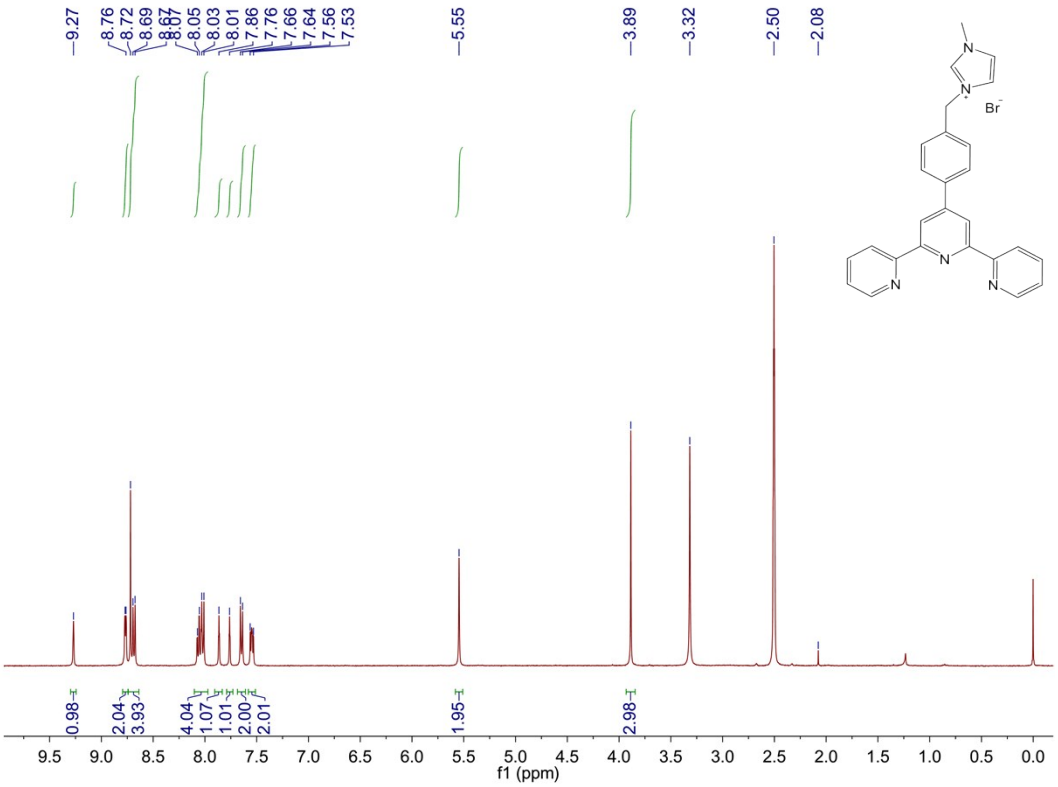

Fig. S3 ^{1}H NMR spectrum (400 MHz, DMSO-d6) of compound **1** at 298 K.

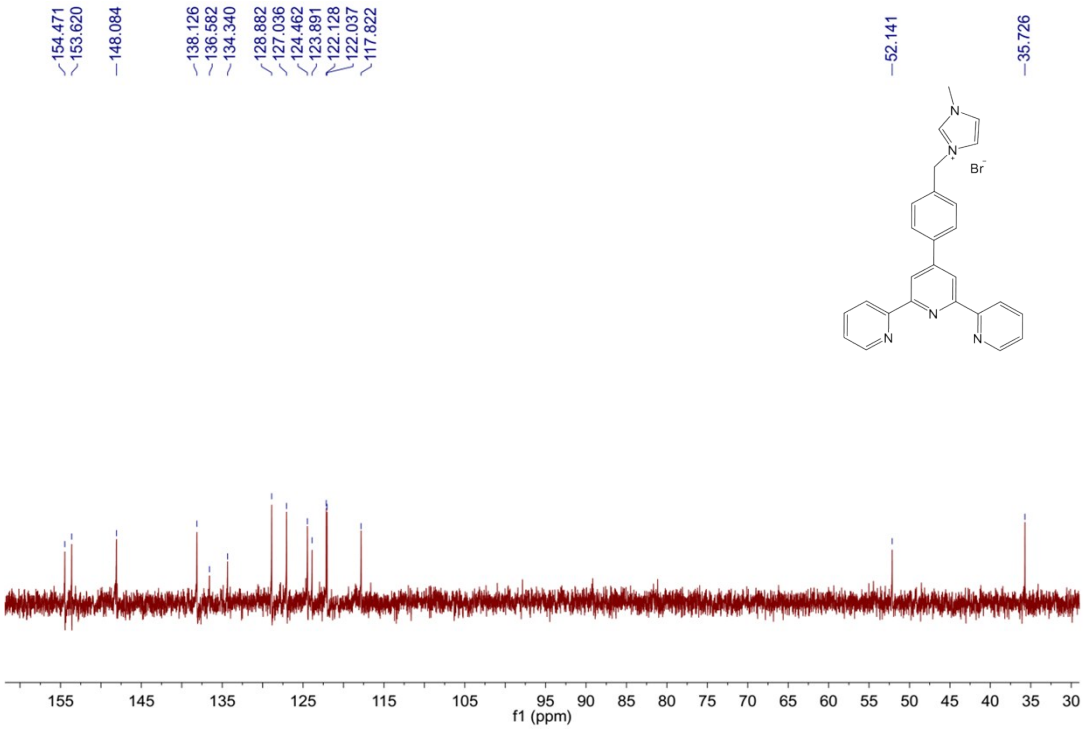

Fig. S4 ^{13}C NMR spectrum (400 MHz, DMSO-d_6) of compound **1** at 298 K**.**

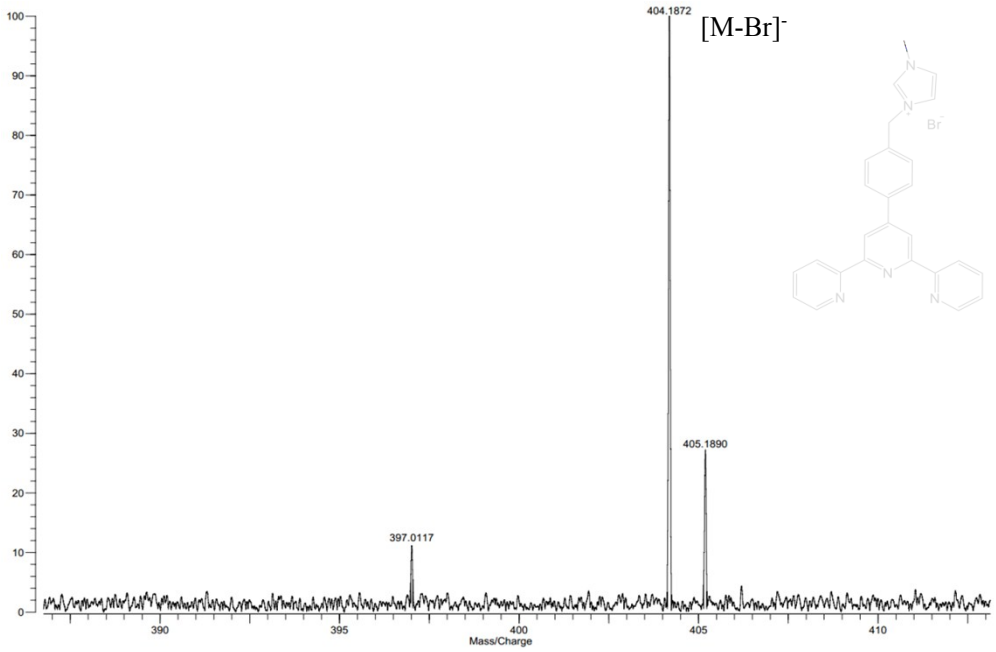

Fig. S5 The ESI-MS spectrum of compound **1**.

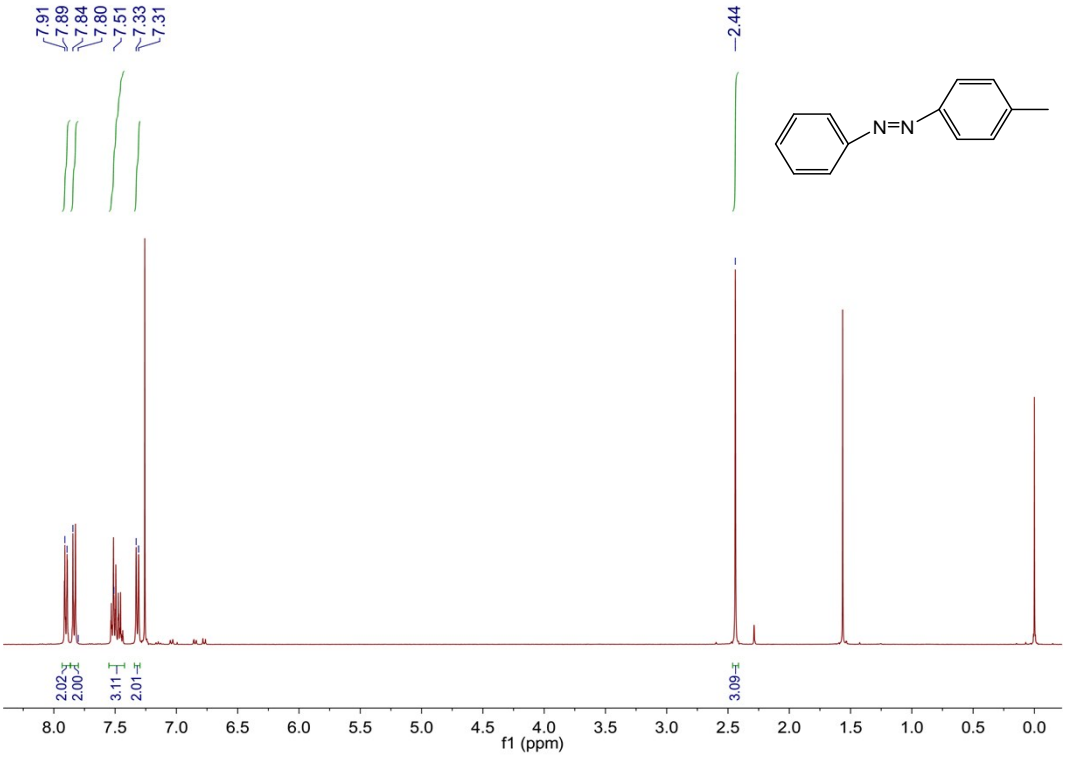

Fig. S6 ^{1}H NMR spectrum (400 MHz, $CDCl_3$-d_6) of compound **C** at 298 K.

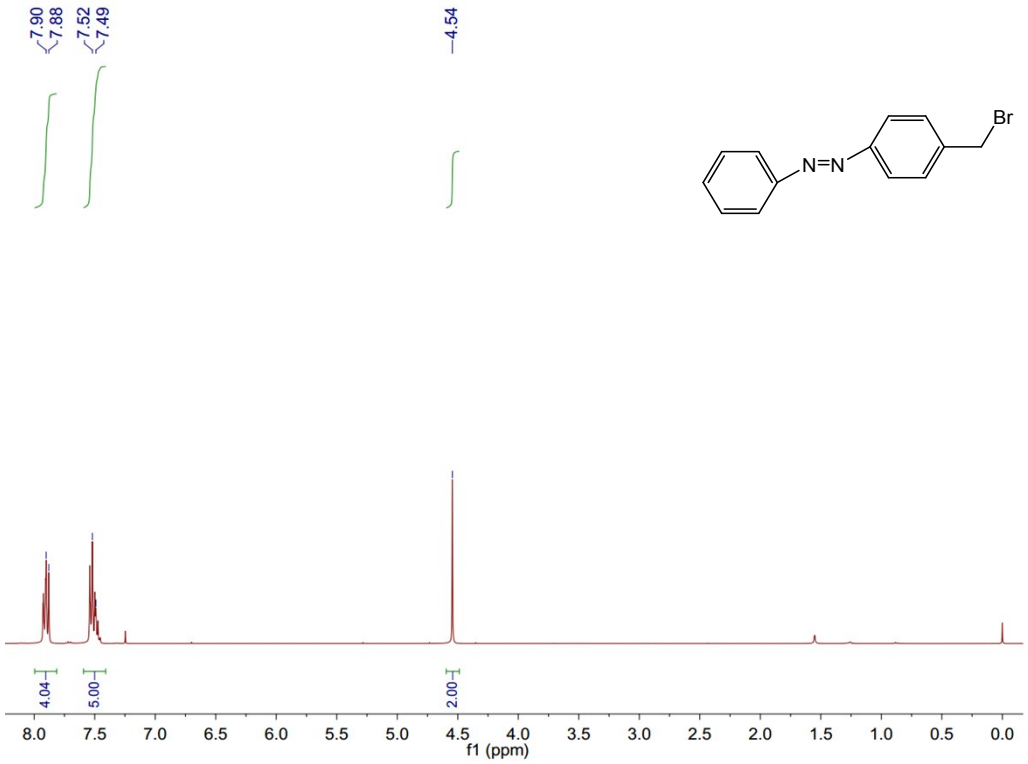

Fig. S7 ^{1}H NMR spectrum (400 MHz, $CDCl_3$-d_6) of compound **D** at 298 K.

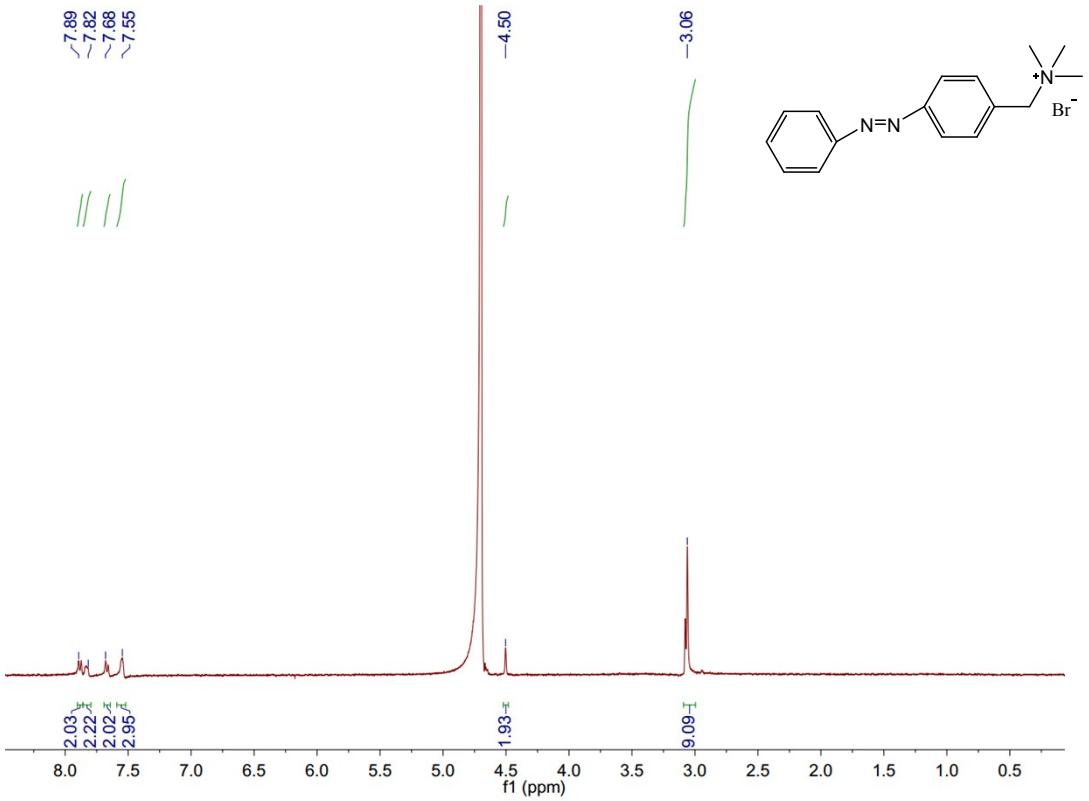

Fig. S8 ^{1}H NMR spectrum (400 MHz, D_2O) of compound *E*-**2** at 298 K.

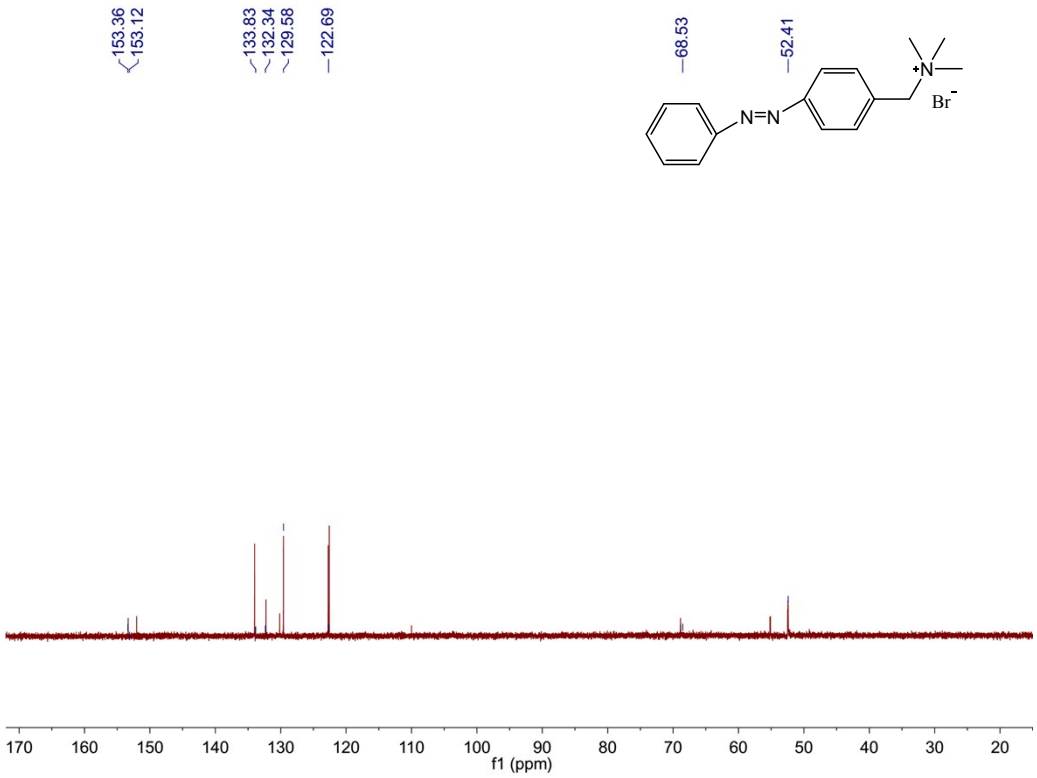

Fig. S9 ^{13}C NMR spectrum (400 MHz, D_2O) of compound *E*-**2** at 298 K.

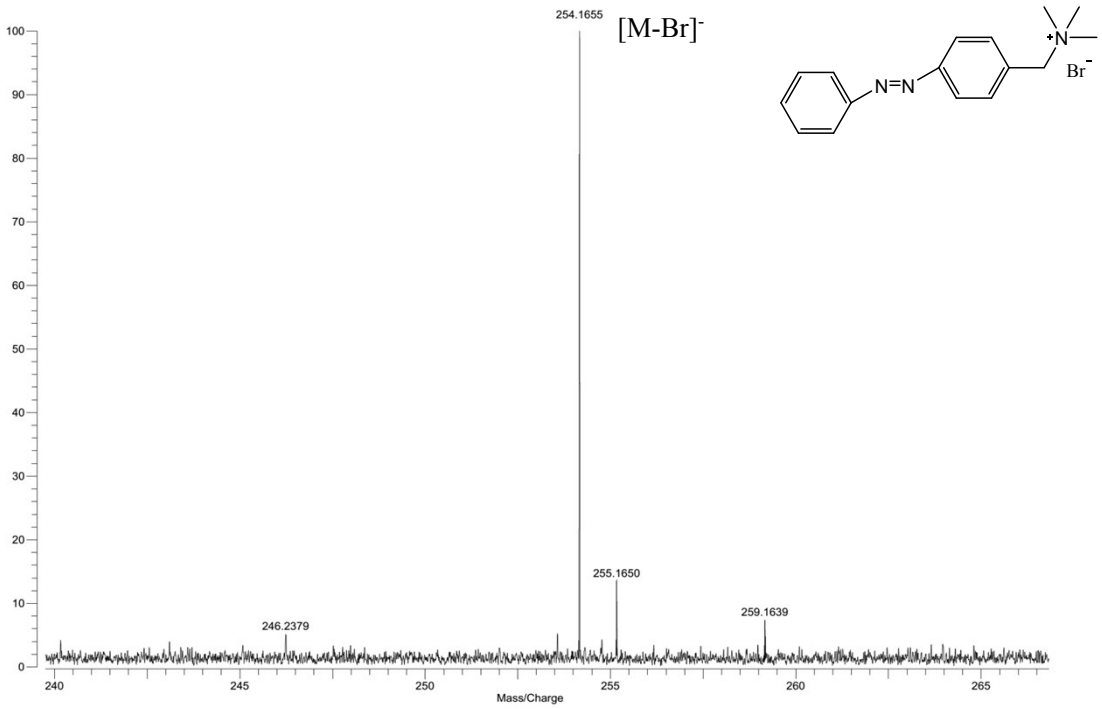

Fig. S10 The ESI-MS spectrum of compound *E*-**2**.

4. Characterizations of the compounds.

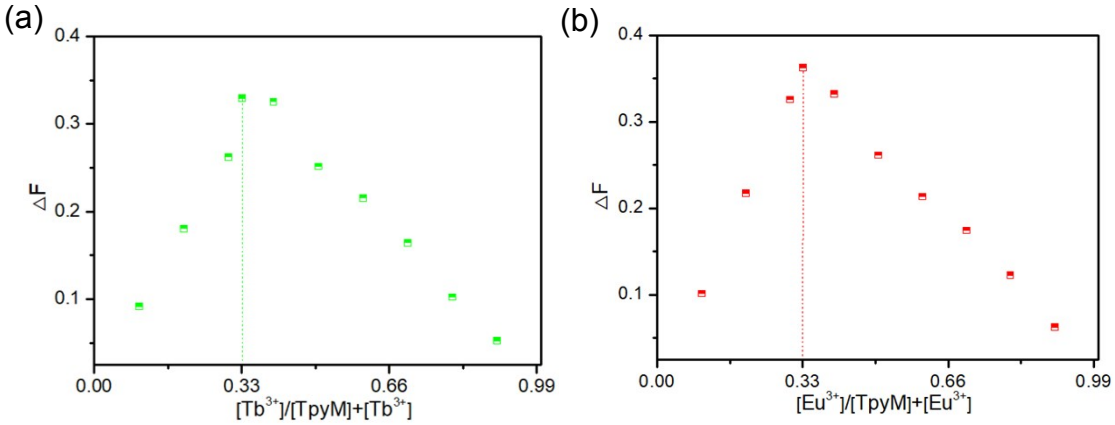

Fig. S11 Job plot for host molecular **1** with (a) $Tb(NO_3)_3 \cdot 6H_2O$ and (b) $Eu(NO_3)_3 \cdot 6H_2O$. Absorption changes recorded at 275 nm for **1** . The sum of the total concentrations of hosts and guests is constant (0.05 mM) in $CHCl_3/CH_3CN$ (1:1, v/v) solution.

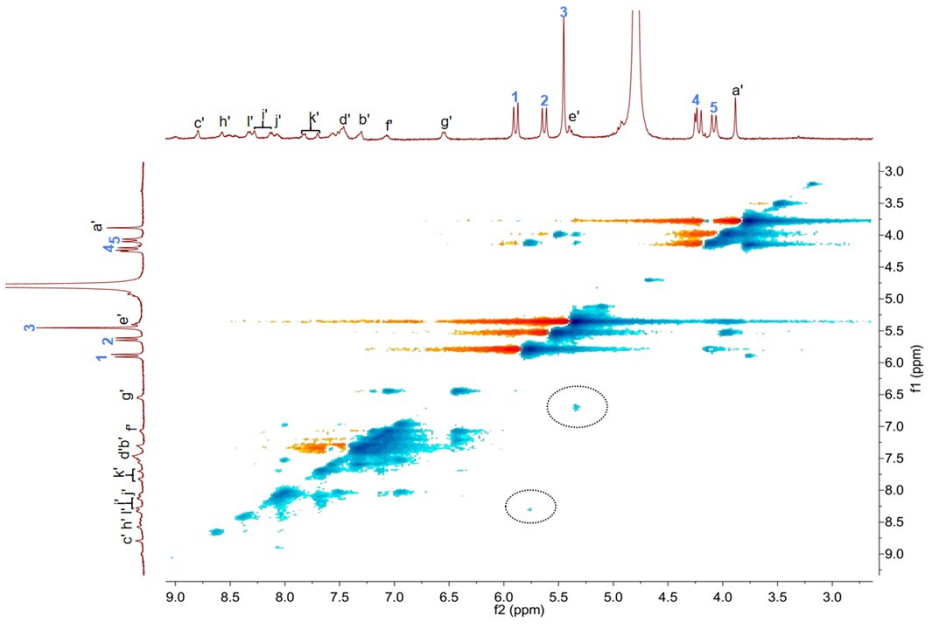

Fig. S12 ^1H-^1H NOESY spectrum of CB[8]-**1** nanofibers. (3 mM) (400 MHz, D_2O, 298K).

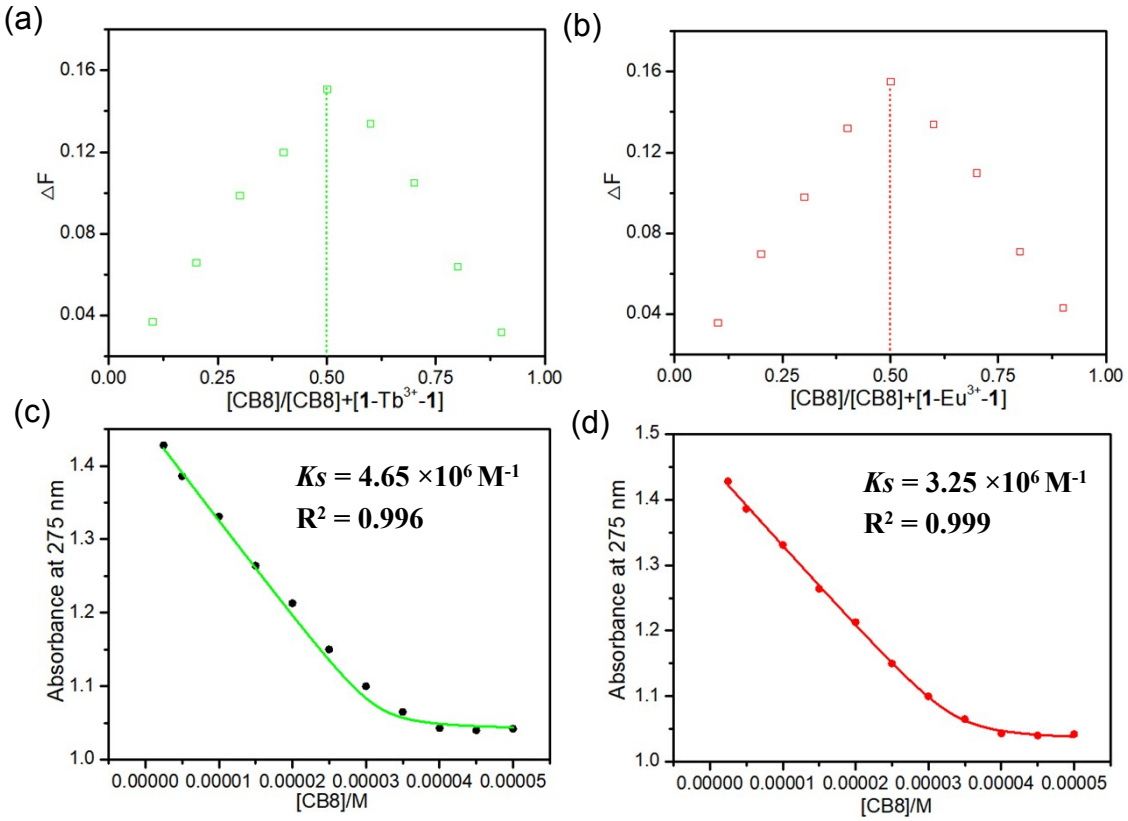

Fig. S13 Job plot for host molecular CB[8] with (a) **1**-Tb^{3+}-**1** and (b) **1**-Eu^{3+}-**1** Absorption changes recorded at 275 nm. The sum of the total concentrations of hosts and guests is constant (0.05 mM) in aqueous solution. The nonlinear least-squares analysis of absorbance's variation of (c) **1**-Tb^{3+}-**1** and (d) **1**-Eu^{3+}-**1** (0.025 mM) with the concentration of CB[8] (0.025 mM) to calculate the binding constant, in aqueous solution at 25 °C.

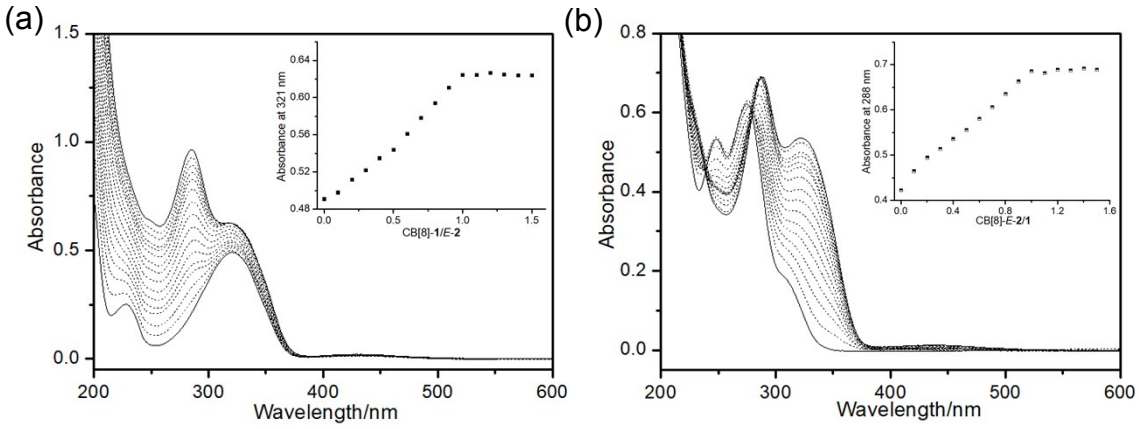

Fig. S14 Alternation of UV-vis spectra of (a) *E*-**2** (0.025 mM) upon addition of CB[8]-**1** (0.025 mM) from 1:0 to 1:1.5, and (b) **1** (0.025 mM) upon addition of CB[8]-*E*-**2** (0.025 mM) from 1:0 to 1:1.5, in aqueous solution at 25 °C. Inset:The variation of absorbance 321 nm upon addition of CB[8]-**1** and 288 nm upon addition of CB[8]-*E*-**2**.

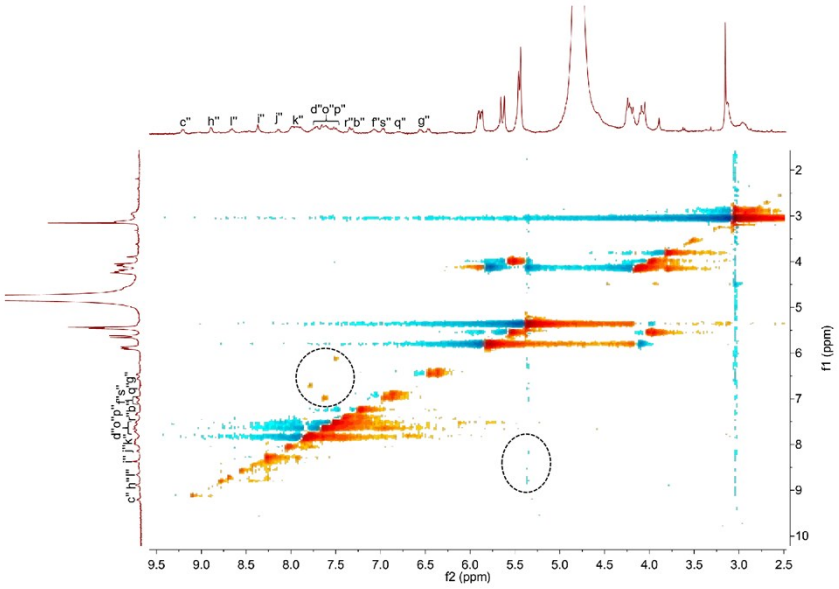

Fig. S15 ^{1}H-^{1}H ROESY spectrum of 1:1:1 equimolar mixture of CB[8]-**1**-*E*-**2** (3 mM) (400 MHz, D_2O, 298K).

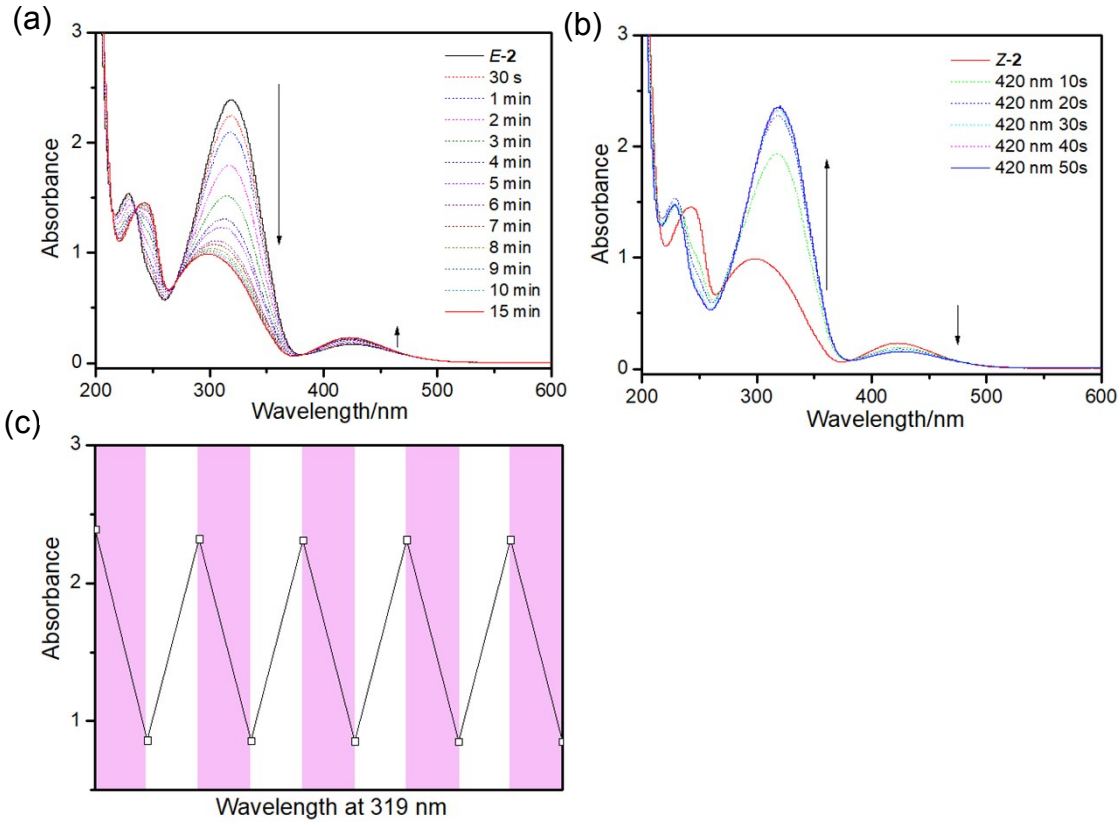

Fig. S16 UV-Vis absorption spectra of (a) *E*-**2** (0.05 mmol) solution under UV irradiation at 365 nm. (b) *Z*-**2** after visible irradiation at 420 nm. (c) UV-Vis absorption at 319 nm of *E*-**2** observed upon several cycles under irradiation at 365 nm (pink) for 10 min and irradiation at 420 nm (white) for 1 min.

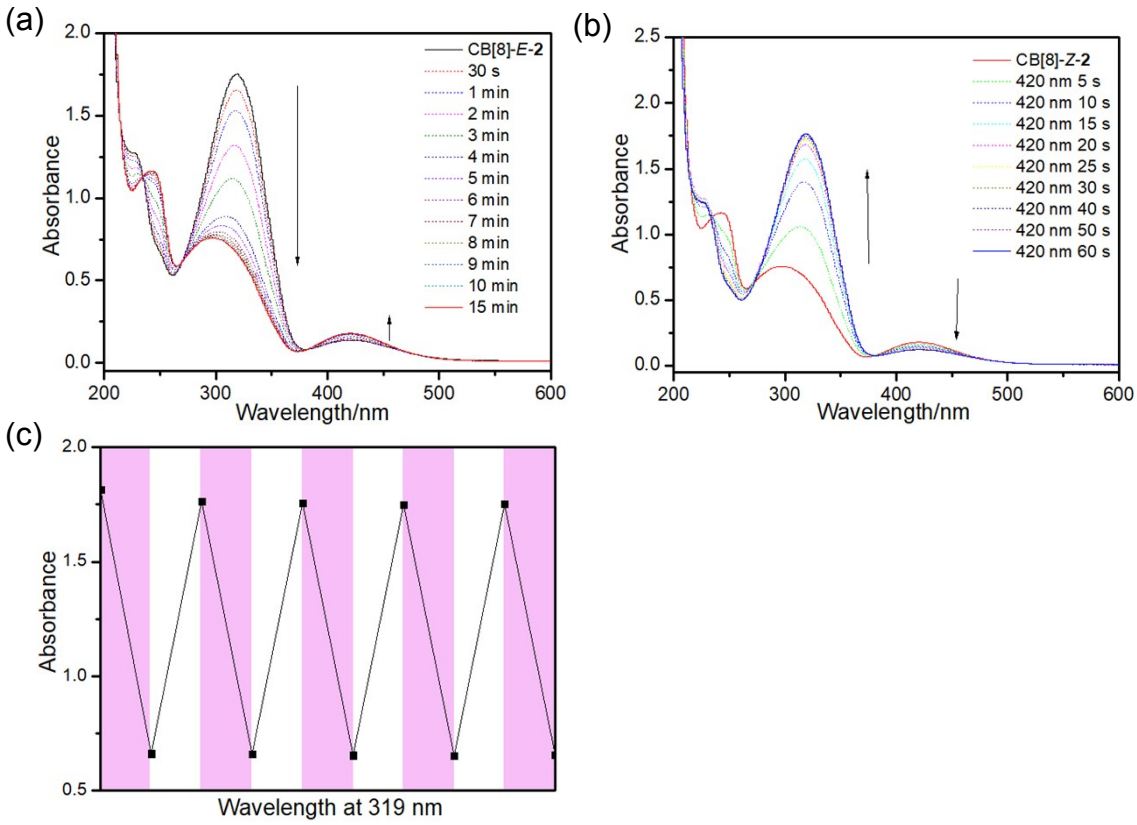

Fig. S17 UV-Vis absorption spectra of (a) CB[8]-*E*-**2** (0.05 mmol, molar ratio, 1:2) solution under UV irradiation at 365 nm. (b) CB[8]-*Z*-**2** after visible irradiation at 420 nm. (c) UV-Vis absorption at 319 nm of CB[8]-*E*-**2** observed upon several cycles under irradiation at 365 nm (pink) for 10 min andirradiation at 420 nm (white) for 1 min.

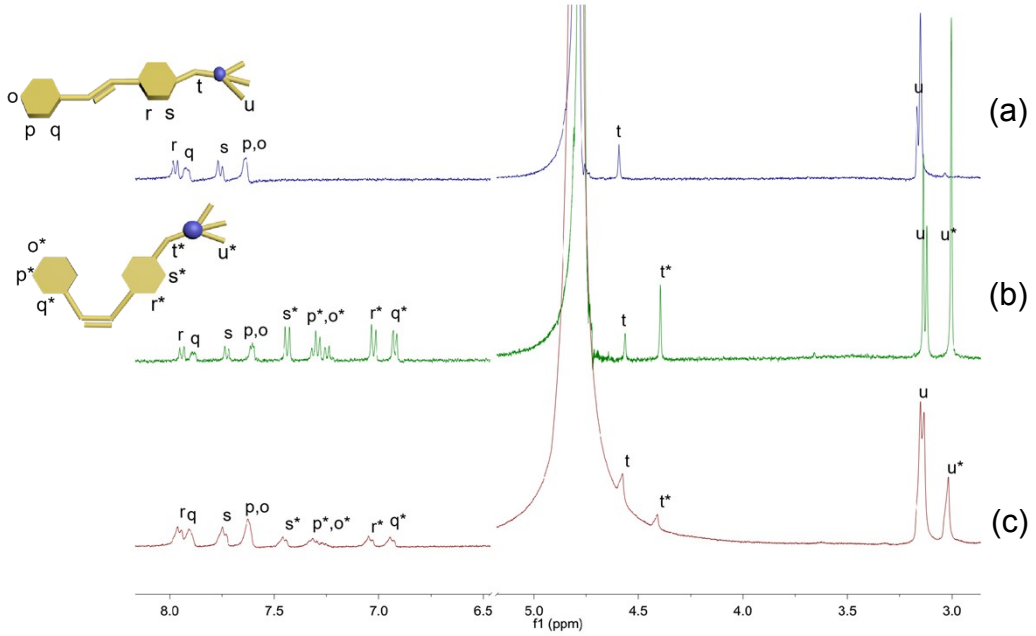

Fig. S18 Partial ^{1}H NMR spectra (400 MHz, D_2O, 298K) of (a) 1.00 mM *E*-**2**, (b) after irradiation at 365 nm for 10 min (c) and then after further irradiation at 420 nm for 1 min.

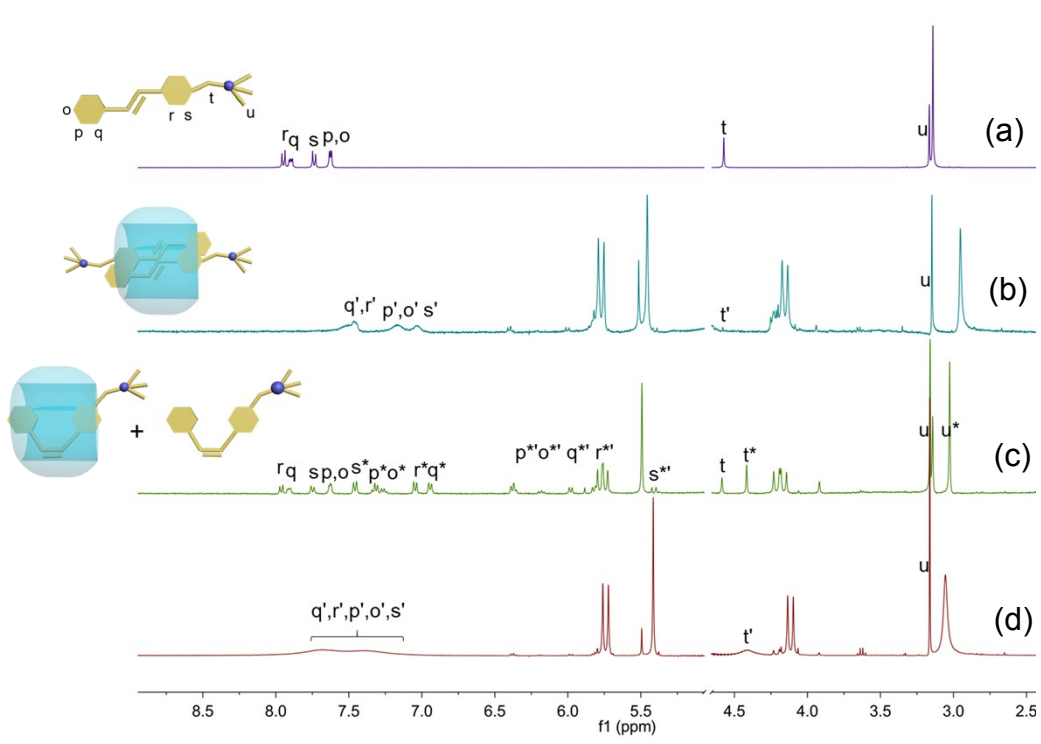

Fig. S19 Partial ^{1}H NMR spectra (400 MHz, D_2O, 298K) of (a) 1.00 mM *E*-**2**, (b) 1.00 mM CB[8]-*E*-**2** (1:2), (c) after irradiation at 365 nm for 10 min (d) and then after further irradiation at 420 nm for 1 min.

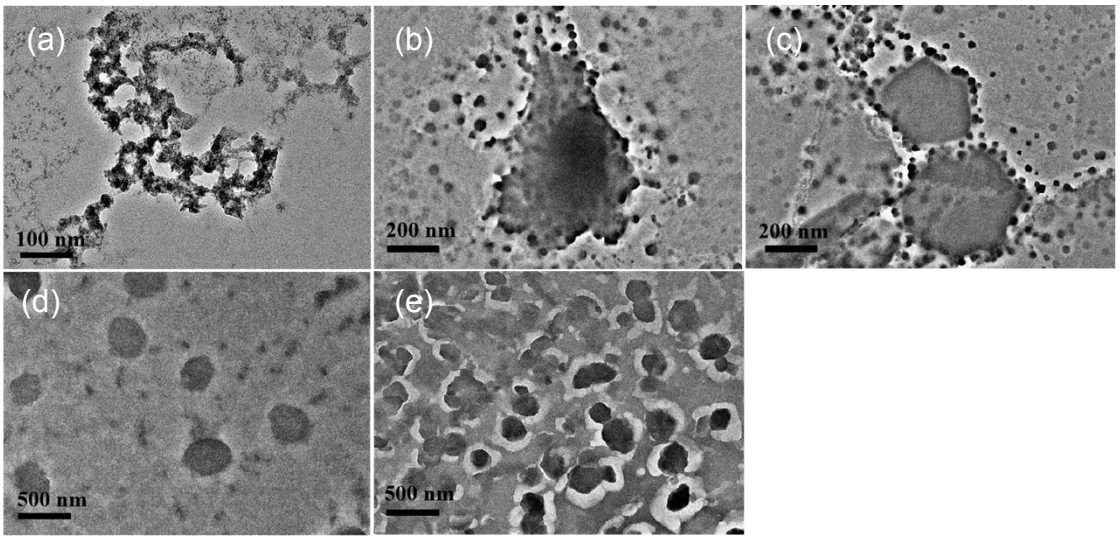

Fig. S20 TEM images of the CB[8]-**1**-*E*-**2** assembly with (a) 0 equiv SLS, (b) 6 equiv SLS, (c) 12 equiv SLS, (d) 18 equiv SLS, (e) 30 equiv SLS.

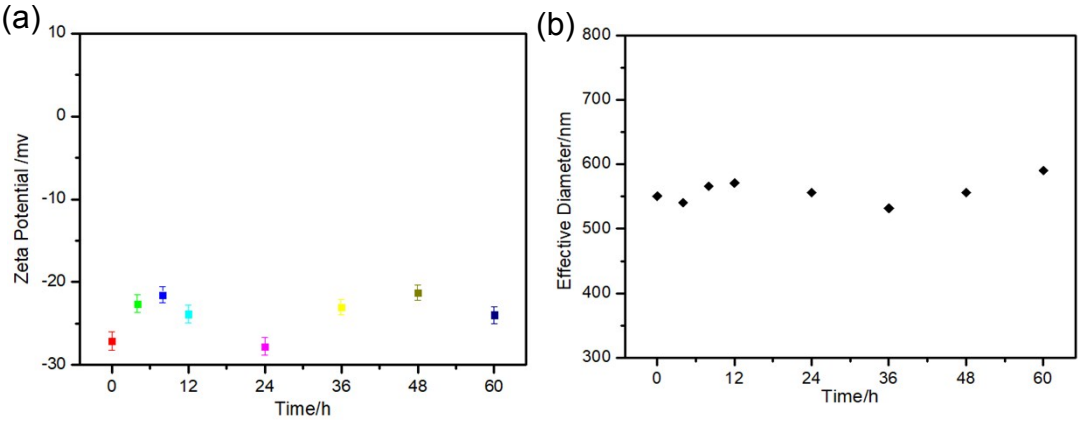

Fig. S21 (a) The zeta potential and (b) DLS date of CB[8]-**1**-*E*-**2**/SLS (1:18) at 0 h, 4 h, 8 h, 12 h, 24 h, 36 h, 48 h and 60 h.

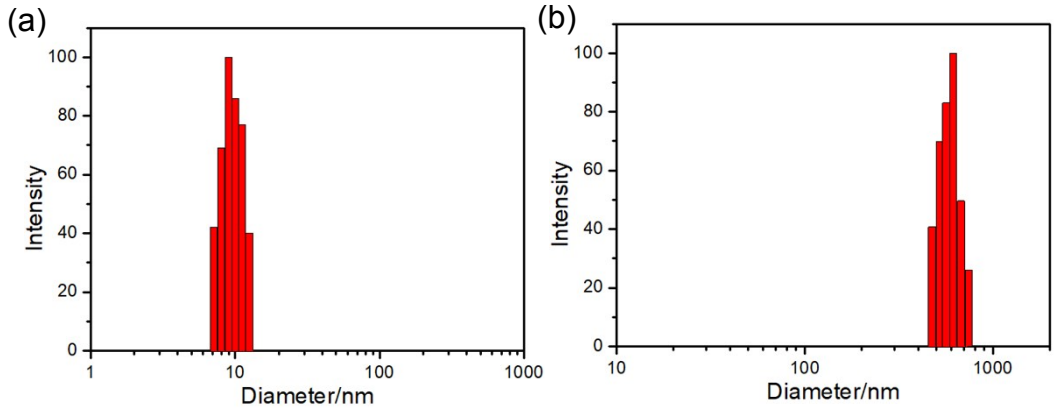

Fig. S22 The DLS data of CB[8]-**1**-*E*-**2**/SLS (1:18) 2D supramolecular assembly (a) after irradiation at 365 nm for 10 min and (b) then after further irradiation at 420 nm for 1 min.

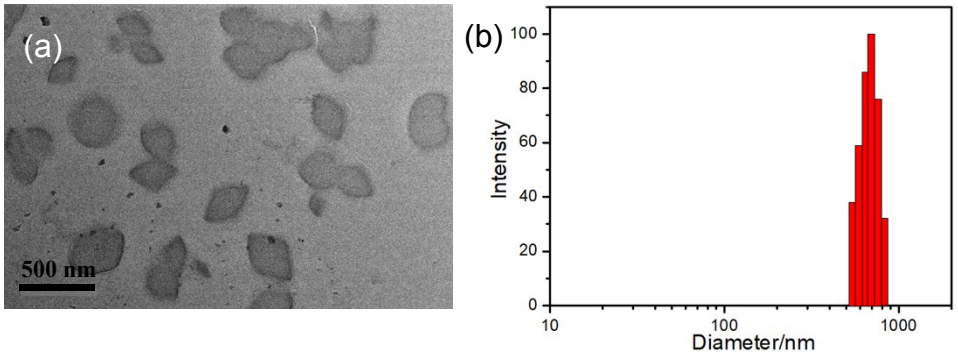

Fig. S23 TEM image and DLS data of DOX-CB[8]-**1**-*E*-**2**/SLS in deionized water.

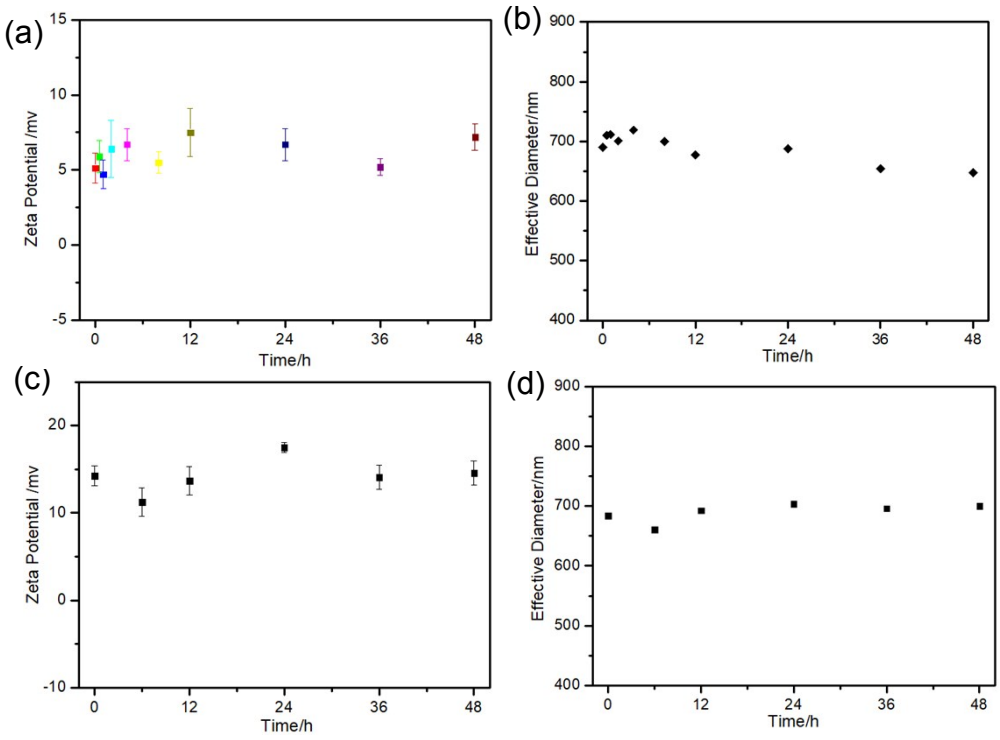

Fig. S24 The zeta potentials (a, c) and DLS data (b, d) of DOX-CB[8]-**1**-*E*-**2**/SLS in water and pH 7.4 PBS, respectively.

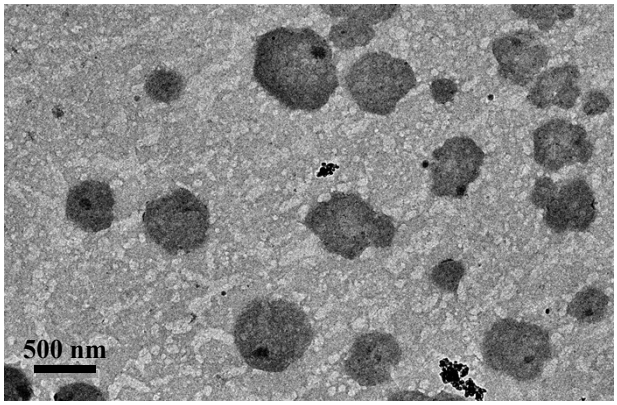

Fig. S25 TEM image of DOX-CB[8]-**1**-*E*-**2**/SLS in pH 7.4 PBS.

5. Cell experiment.

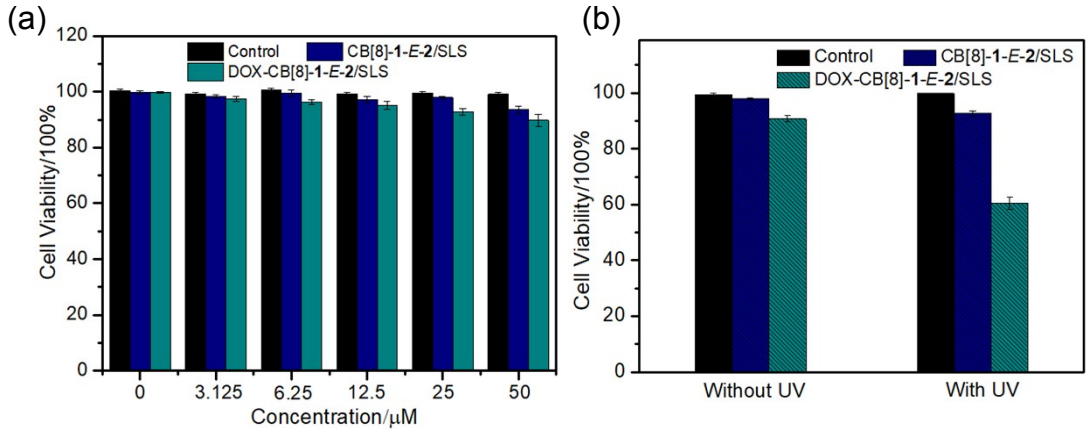

Fig. S26 (a) MTT cell viability assay of CB[8]-**1**-*E*-**2**/SLS and DOX-CB[8]-**1**-*E*-**2**/SLS nanosheets on human L02 cells for 24 h incubation. (b) Cell viability of HeLa cells incubated with 50 μM CB[8]-**1**-*E*-**2**/SLS and DOX-CB[8]-**1**-*E*-**2**/SLS nanosheets without or with UV light irradiation for 30 min (365 nm, 1 W cm^{-2}).

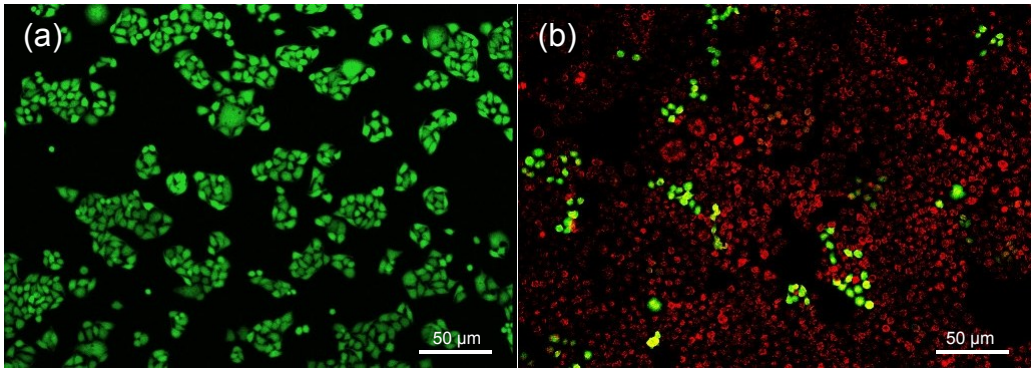

Fig. S27 Fluorescence images of calcein-AM and PI-stained HeLa cells (a), and (b) incubated with DOX-CB[8]-**1**-*E*-**2**/SLS with UV light irradiation for 30 min (365 nm, 1 W cm^{-2}).

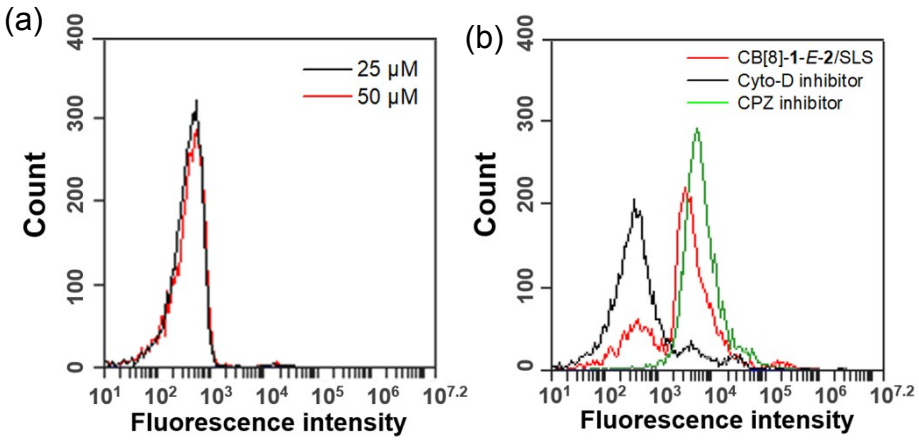

Fig. S28 Flow cytometry histograms illustrating the internalization mechanism of supramolecular nanosheets. (a) Flow cytometry analysis of the HeLa cells incubated with 25 μM/50 μM CB[8]-1-*E*-2/SLS nanosheets. (b) Flow cytometry analysis of the e□ect of endocytosis inhibitors on cellular uptake of the nanosheets.

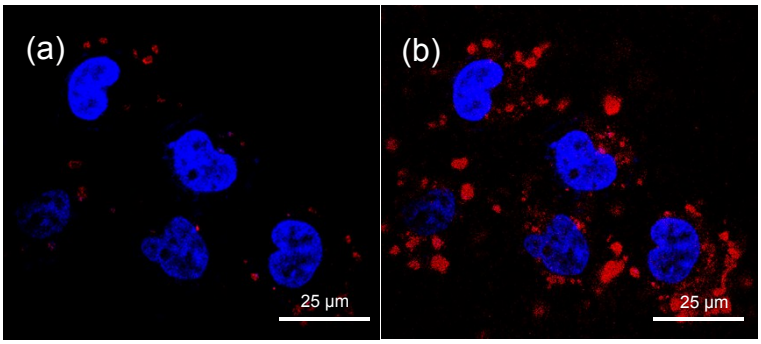

Fig. S29 CLSM images of DOX-CB[8]-**1**-*E*-**2**/SLS nanosheets in HeLa cells before (a) and after (b) UV light irradiation for 30 min (365 nm, 1 W cm^{-2}).